Viscous properties of isotropic fluids composed of linear molecules: Departure from the classical Navier-Stokes theory in nano-confined geometries

J. S. Hansen*
Centre for Molecular Simulation, Swinburne University of Technology, P.O. Box 218, Hawthorn, Victoria 3122, Australia

Peter J. Daivis†
Applied Physics, School of Applied Sciences, RMIT University, GPO Box 2476, Melbourne, Victoria 3001, Australia

B. D. Todd‡
Centre for Molecular Simulation, Swinburne University of Technology, P.O. Box 218, Hawthorn, Victoria 3122, Australia
(Received 21 May 2009; published 28 October 2009)

In this paper we present equilibrium molecular-dynamics results for the shear, rotational, and spin viscosities for fluids composed of linear molecules. The density dependence of the shear viscosity follows a stretched exponential function, whereas the rotational viscosity and the spin viscosities show approximately power-law dependencies. The frequency-dependent shear and spin viscosities are also studied. It is found that viscoelastic behavior is first manifested in the shear viscosity and that the real part of the spin viscosities features a maximum for nonzero frequency. The calculated transport coefficients are used together with the extended Navier-Stokes equations to investigate the effect of the coupling between the intrinsic angular momentum and linear momentum for highly confined fluids. Both steady and oscillatory flows are studied. It is shown, for example, that the fluid flow rate for Poiseuille flow is reduced by up to 10% in a 2 nm channel for a buta-triene fluid at density 236 kg m^{-3} and temperature 306 K. The coupling effect may, therefore, become very important for nanofluidic applications.

DOI: 10.1103/PhysRevE.80.046322 PACS number(s): 47.61.−k, 05.60.−k, 47.10.−g, 66.20.Gd

I. INTRODUCTION

It is well known that the internal molecular degrees of freedom couple to the system's macroscopic fluid dynamical quantities such as the streaming velocity [1–3]. A complete fluid dynamical description should, therefore, at least in principle, include these internal degrees of freedom. According to Evans and Hanley [4] it was Born [5] who first discussed the coupling between intrinsic angular momentum caused by the molecular rotation and the fluid's translational motion. Grad [6] and later Snider and Lewchuck [3] treated the problem via irreversible thermodynamics and Curtiss [1] applied kinetic theory using a rather involved analysis of the Boltzmann equation. In this work the balance equations were deduced for both the isotropic and anisotropic cases. de Groot and Mazur [2], on the other hand, treated the isotropic problem exclusively also ignoring the effect of intrinsic angular velocity gradients in the fluid. Finally, Ailawadi *et al.* [7] investigated the isotropic problem via statistical mechanics and were able to derive the fluctuation formulae for the transport coefficients. In the last two decades quite a lot of attention has been given to identifying and evaluating the relevant transport coefficients in the anisotropic nematic phase; see, for example, Refs. [8–11]. Travis *et al.* [12,13] and Delhommelle and Evans [14] used molecular-dynamics simulations to study diatomic molecular fluids undergoing steady Poiseuille flow. They showed that the angular velocity profile agreed with continuum predictions. Hansen *et al.* [15,16] performed the same simulations but for an oscillatory flow and they concluded that for diatomic fluids, where the angular velocity gradient could be ignored, the coupling is in fact negligible due to the very low moment of inertia of the molecules comprising the fluid. However, for larger molecules and for very high degrees of confinement the coupling becomes important depending on the oscillatory frequency.

In recent years the field of nanofluidics has attracted a lot of attention due to its many potential applications. For example, is it believed that carbon nanotubes with diameters of the order of nanometers will play an important role in fabrication of membranes for desalination of water [17]. As mentioned above, for such confining geometries the fluid dynamics may be affected by the molecular rotation. In fact, for ferrofluids the rotation plays an essential role in the dynamics of the system; see, e.g., Ref. [18]. To our knowledge no one has yet performed an investigation of the effect confinement has on isotropic molecular fluids composed of simple linear molecules. Such investigation should include the coupling between the intrinsic angular momentum and translational momentum allowing for nonzero angular velocity gradients. One reason for this is perhaps that the dynamical properties of such system are characterized by four transport coefficients for incompressible fluids. In this paper we will use a series of equilibrium molecular-dynamics simulations to calculate these coefficients for different fluids and state points. This then enables us to accurately calculate the effect of the coupling.

The paper is organized as follows: in the next section we will write down the governing continuum hydrodynamical equations for the angular momentum and linear momentum.

*jehansen@swin.edu.au
†peter.daivis@rmit.edu.au
‡btodd@swin.edu.au

In Sec. III we will explain the methodology used to evaluate the transport coefficients. The results are presented in Sec. IV and the effect of the coupling is discussed in Sec. V. The last section is devoted to the conclusion and a few final remarks.

II. GOVERNING CONTINUUM EQUATIONS

The extended Navier-Stokes equations for molecular fluids that include the coupling between the molecular internal angular momentum per unit mass, **s**, and the streaming velocity, **u**, are well known. We will not go into details here with the derivation but refer the reader to Refs. [2,3,19]. The equations are given here as

$$\rho\frac{D\mathbf{u}}{Dt} = \rho\mathbf{F}_e - \nabla p + (\eta_v + \eta_0/3 - \eta_r)\nabla(\nabla\cdot\mathbf{u}) + (\eta_0 + \eta_r)\nabla^2\mathbf{u} + 2\eta_r(\nabla\times\boldsymbol{\Omega}), \tag{1}$$

$$\rho\frac{D\mathbf{s}}{Dt} = \rho\boldsymbol{\Gamma} + 2\eta_r(\nabla\times\mathbf{u} - 2\boldsymbol{\Omega}) + (\zeta_v + \zeta_0/3 - \zeta_r)\nabla(\nabla\cdot\boldsymbol{\Omega}) + (\zeta_0 + \zeta_r)\nabla^2\boldsymbol{\Omega}, \tag{2}$$

where ρ is the mass density, $\mathbf{F}_e$ and $\boldsymbol{\Gamma}$ are the applied external force and torque per unit mass, η_0, η_v, and η_r are the shear, bulk, and rotational viscosities, respectively, ζ_0, ζ_v, and ζ_r are the corresponding spin viscosities, and $\boldsymbol{\Omega}$ is the streaming intrinsic angular velocity. We assume that all the transport coefficients are constant and wave vector independent. Now, consider the situation where the fluid is composed of uniaxial rigid molecules. For such molecular fluids the angular momentum can be written as [12]

$$\mathbf{s} = \Theta\boldsymbol{\Omega}, \tag{3}$$

where Θ is 1/3 of the trace of the moment of inertia tensor per unit mass. If at time $t=0$ the fluid is perturbed by, say, $u_x(y,t=0)=u'\delta(y-y_0)$, where u' is sufficiently small such that the convection term can be ignored and $-\infty<y<\infty$, the relaxation is governed by the linearized Navier-Stokes equations:

$$\rho\frac{\partial u_x(y,t)}{\partial t} = (\eta_0 + \eta_r)\frac{\partial^2 u_x(y,t)}{\partial y^2} + 2\eta_r\frac{\partial\Omega_z(y,t)}{\partial y}, \tag{4}$$

$$\rho\Theta\frac{\partial\Omega_z(y,t)}{\partial t} = -2\eta_r\left[\frac{\partial u_x(y,t)}{\partial y} + 2\Omega_z(y,t)\right] + (\zeta_0 + \zeta_r)\frac{\partial^2\Omega_z(y,t)}{\partial y^2}. \tag{5}$$

It should be noted that only the transverse component of $\boldsymbol{\Omega}$ will be excited for small u'. This system can readily be solved in Fourier space where the equations read

$$\rho\frac{\partial\tilde{u}_x(k_y,t)}{\partial t} = -(\eta_0 + \eta_r)k_y^2\tilde{u}_x(k_y,t) + i2\eta_r k_y\tilde{\Omega}_z(k_y,t),$$

$$\rho\Theta\frac{\partial\tilde{\Omega}_z(k_y,t)}{\partial t} = -2\eta_r[ik_y\tilde{u}_x(k_y,t) + 2\tilde{\Omega}_z(k_y,t)] - (\zeta_0 + \zeta_r)k_y^2\tilde{\Omega}_z(k_y,t). \tag{6}$$

It is possible to turn this into an algebraic equation using a Laplace transform as well; however, for our purpose we will simply discuss the solution of Eq. (6). Equation (6) is simply a linear differential equation system in which the dynamics is governed by two eigenvalues that can be found by solving the equation

$$\begin{vmatrix} -(\eta_0 + \eta_r)k_y^2/\rho - \lambda & 2\eta_r ik_y/\rho \\ 2\eta_r ik_y/\rho\Theta & -[4\eta_r + (\zeta_0 + \zeta_r)k_y^2]/\rho\Theta - \lambda \end{vmatrix} = 0. \tag{7}$$

From this it can be seen that the eigenvalues have a nontrivial dispersion relation; i.e., λ_1 and λ_2 are dependent on k_y. The dispersion relation can be Taylor expanded around $k_y=0$ giving

$$\lambda_1 = -\frac{4\eta_r}{\rho\Theta} - \sum_{n=1}^{\infty} a_{2n}k_y^{2n}, \quad \lambda_2 = -\sum_{n=1}^{\infty} a_{2n}k_y^{2n}, \tag{8}$$

where the coefficients a_l are functions of the transport coefficients and the moment of inertia. From Eq. (8) we see that there exists a mode which is independent of the wave vector. This local fast mode is due to the intrinsic molecular angular momentum relaxation and can also be derived from the relaxation of the longitudinal component Ω_y. Another very interesting point to note is that the dispersion relations also show the existence of higher wave-vector modes, thus, in the hydrodynamic regime where $k_y \ll 1$ the relaxation is slower than a simple diffusive process which is on the order of k_y^2 [20]. This is a direct effect of the coupling between the intrinsic angular and translational momenta. From the dispersion relation we can define an intrinsic relaxation time τ [2] or characteristic frequency ω_c [16]:

$$\tau = \frac{1}{\omega_c} = \frac{\rho\Theta}{4\eta_r}. \tag{9}$$

Also, it is possible to define a characteristic length,

$$l_c = \left[\frac{\zeta_0 + \zeta_r}{\eta_r}\right]^{1/2}, \tag{10}$$

which qualitatively indicates on what length scale spin diffusion becomes important relative to the spin relaxation.

As mentioned in Sec. I, de Groot and Mazur did not include the diffusion term in Eq. (5). The rate of change of the angular momentum is then only dependent on the local exchange between vorticity and angular momentum. Thus, if the spin diffusion term is negligible then for a steady incompressible flow where $\boldsymbol{\Gamma}=\mathbf{0}$, we obtain from Eq. (2):

$$\boldsymbol{\Omega} = \frac{1}{2}\nabla\times\mathbf{u}. \tag{11}$$

Substituting this into Eq. (1) we see that the streaming velocity is decoupled from the molecular rotation, that is, for steady flows where the angular momentum diffusion is neglected no coupling effect is present. Hansen *et al.* [16] solved the problem for oscillatory flows where the coupling effect persists. They proposed a dimensionless number to estimate the coupling effect from the molecular rotation in the absence of angular velocity gradients:

$$\varepsilon = \frac{\Theta \nu_0}{h}\left[\frac{\omega}{\nu_r^3}\right]^{1/2}, \tag{12}$$

where h is the radius of the tube and ν_0 and ν_r are the kinematic viscosities, i.e., $\nu_0=\eta_0/\rho$ and $\nu_r=\eta_r/\rho$. For $\varepsilon \approx 1 \times 10^{-3}$ the flow rate is reduced by around 1% [16]. Furthermore, for oscillatory flows large coupling effects can then be expected for frequencies around ω_c, Eq. (9).

III. METHODOLOGY

The molecular model applied here includes pair interaction, bond stretching, and bending. The potential energy for the system thus reads

$$U = \sum_{\text{pairs}} U_p(r_{ab}) + \sum_{\text{bonds}} U_b(r_{ab}) + \sum_{\text{angles}} U_a(\theta), \tag{13}$$

where r_{ab} is the distance between united atomic units (UAU) a and b, and θ is the angle between two chemical bonds connected to the same UAU. U_p is the pair potential given by the truncated and shifted Lennard-Jones potential,

$$U_p(r_{ab}) = \begin{cases} 4\epsilon\left[\left(\frac{\sigma}{r_{ab}}\right)^{12} - \left(\frac{\sigma}{r_{ab}}\right)^{6}\right] - U_p(r_c) & \text{if } r_{ab} \le r_c \text{ and } a \in i, b \notin i \\ 0 & \text{otherwise,} \end{cases} \tag{14}$$

where i represents molecule index; i.e., UAU a and b only interact if they belong to different molecules. σ is a length scale and ϵ is an energy scale. The critical cutoff, r_c, is set to 2.5σ. The bond stretching potential is given by a simple spring potential:

$$U_b(r_{ab}) = \frac{1}{2}k_s(r_{ab} - l_b)^2, \tag{15}$$

where k_s is the spring force constant and l_b is the mean (or equilibrium) bond length. Unless otherwise stated we shall use $l_b=0.3526\sigma$. The spring force constant for a carbon-carbon double bond is around 690 kcal mol^{-1} Å^{-2} [21]. Including such large forces into the molecular-dynamics simulations will demand very small time steps possibly leaving the method useless. However, when evaluating the transport properties one needs only ensure that the bonds are sufficiently stiff; see Refs. [22,23] and references therein. We will here use $k_s=2\times10^4\epsilon\sigma^{-2}$, which is around four times smaller than the spring constant for the carbon-carbon double bond. The bending potential used is that typically applied for alkanes [24,25]:

$$U_a(\theta) = \frac{1}{2}k_\theta[\cos(\theta) - \cos(\theta_0)]^2, \tag{16}$$

where $\theta_0=\pi$ is the equilibrium bending angle for linear molecules and $k_\theta=1\times10^4\epsilon$ is the bending constant.

One can express any mechanical quantity in terms of ϵ, σ and mass m. In this way mass density is given as $\rho^*=\rho\sigma^3/m$, temperature is $T^*=k_BT/\epsilon$, time is $t^*=(\epsilon/m\sigma^2)^{1/2}t$, pressure is $p^*=p\sigma^3/\epsilon$, and torque is $\tau^*=\tau/\epsilon$ and so forth [26]. We shall apply these dimensionless units and drop the asterisk all together in this and the following section. In Sec. V we will return to normal physical units unless otherwise stated.

Initially, the system is equilibrated to a desired atomic temperature of $T_a=4.25$ using a Nosé-Hoover thermostat [27,28]. After equilibration the thermostat is switched off and the rest of the simulation is carried out in the *NVE* ensemble. The choice of ensemble is a matter of convenience. The equations of motion are integrated forward in time using the leap-frog method [26] with time step of $\Delta t=0.001$. It is important to note here that the molecular temperature T_m defined as

$$T_m = \frac{\Sigma \mathbf{p}_i^2/m_i}{(3N_{\text{mol}} - 3)k_B}, \tag{17}$$

where $\mathbf{p}_i$ is the molecular center-of-mass peculiar momentum and N_{mol} is the number of molecules, is the same as T_a due to equipartition. We will here just use T for the temperature.

During each simulation the molecular pressure tensor, $\mathbf{P}$, and the couple tensor, $\mathbf{Q}$, are calculated. On a microscopic scale the pressure tensor (or momentum flux tensor) is given by [29]

$$\mathbf{P}(t) = \frac{1}{V}\left[\sum_i \frac{\mathbf{p}_i\mathbf{p}_i}{m_i} + \sum_i \sum_{j>i} \mathbf{r}_{ij}\mathbf{F}_{ij}\right], \tag{18}$$

where V is the system volume and $\mathbf{r}_{ij}=\mathbf{r}_i-\mathbf{r}_j$, where $\mathbf{r}_i$ and $\mathbf{r}_j$ are the center of mass of molecule i and j, respectively. $\mathbf{F}_{ij}$ is the force acting between molecule i and j and is given by

$$\mathbf{F}_{ij} = \sum_{a\in i}\sum_{b\in j}\mathbf{F}_{ab}, \tag{19}$$

where $\mathbf{F}_{ab}$ is the force acting between UAU a in molecule i and UAU b in molecule j. The couple tensor is written as [19]

$$\mathbf{Q}(t) = \frac{1}{V}\left[\sum_i \mathbf{p}_i\mathbf{s}_i + \sum_i\sum_{j>i}\mathbf{r}_{ij}\boldsymbol{\tau}_{ij}\right]. \tag{20}$$

Here $\mathbf{s}_i$ is the angular momentum per unit mass of molecule i and $\boldsymbol{\tau}_{ij}$ is the torque on i due to j, i.e.,

$$\mathbf{s}_i = \frac{1}{m_i}\sum_{a\in i} m_a\mathbf{R}_{ai}\times\mathbf{v}_a \quad \text{and} \quad \boldsymbol{\tau}_{ij} = \sum_{a\in i}\left[\mathbf{R}_{ai}\times\sum_{b\in j}\mathbf{F}_{ab}\right], \tag{21}$$

where $\mathbf{R}_{ai}=\mathbf{r}_a-\mathbf{r}_i$. The tensors $\mathbf{P}$ and $\mathbf{Q}$ can be decomposed into isotropic, traceless, symmetric, and antisymmetric parts, i.e.,

$$\mathbf{P} = p\mathbf{I} + \overset{\text{os}}{\mathbf{P}} + \overset{\text{a}}{\mathbf{P}} \quad \text{and} \quad \mathbf{Q} = q\mathbf{I} + \overset{\text{os}}{\mathbf{Q}} + \overset{\text{a}}{\mathbf{Q}}, \tag{22}$$

where $p=\mathrm{tr}(\mathbf{P})/3$ and $q=\mathrm{tr}(\mathbf{Q})/3$.

It can be shown that for k-dependent processes, e.g., diffusive processes, the corresponding transport coefficient can be found using the conventional Green-Kubo relation [4]. For k-independent processes (or fast modes) the generalized Langevin equation must be solved exactly [30,31]. From the dispersion relation, Eq. (8), we can identify the rotational viscosity to be associated with a fast mode, namely, the intrinsic angular momentum relaxation. To this end, Evans and Hanley [4] have shown that η_r can be found from

$$\tilde{C}_{\eta_r}(s) = \frac{\eta_r s}{s + s^2\tau + 4\eta_r/\rho\Theta}, \tag{23}$$

where τ is a relaxation time and $\tilde{C}_{\eta_r}(s)$ is the Laplace transform of the autocorrelation function of the antisymmetric part of the pressure tensor,

$$\tilde{C}_{\eta_r}(s) = \frac{V}{k_BT}\int_0^\infty C_{\eta_r}(t)e^{-st}ds, \tag{24}$$

where

$$C_{\eta_r}(t) = \langle\overset{\text{a}}{\mathbf{P}}_{\alpha\beta}(0)\overset{\text{a}}{\mathbf{P}}_{\alpha\beta}(t)\rangle \tag{25}$$

and $\alpha\beta$ denotes the xy, xz, or yz off-diagonal tensor element. Since $\tilde{C}_{\eta_r}(s)$ can be found from the molecular-dynamics data it is possible to make a best fit of Eq. (23) to $\tilde{C}_{\eta_r}(s)$. We have observed that both τ and η_r should be used as fitting parameters in order to obtain good results; i.e., τ is not given directly via Eq. (9). The remaining transport coefficients in Eqs. (4) and (5) can be found from the Green-Kubo relations [19]:

$$\frac{k_BT}{V}\eta_0 = \int_0^\infty\langle\overset{\text{os}}{\mathbf{P}}_{\alpha\beta}(0)\overset{\text{os}}{\mathbf{P}}_{\alpha\beta}(t)\rangle dt = \int_0^\infty C_{\eta_0}(t)dt,$$

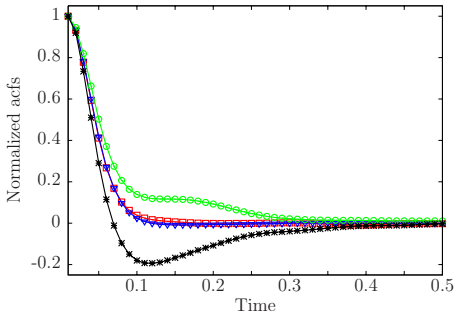

FIG. 1. (Color online) Normalized autocorrelation functions (acfs) at short times for nitrogen where $T=2.14\pm0.06$ and $\rho=1.065$: $C_{\eta_0}(t)$ (circles), $C_{\zeta_0}(t)$ (squares), $C_{\eta_r}(t)$ (stars), and $C_{\zeta_r}(t)$ (triangles). $C_{\eta_0}(0)=73.8\pm1.8$, $C_{\zeta_0}(0)=0.80\pm0.02$, $C_{\eta_r}(0)=1.92\pm0.03$, and $C_{\zeta_r}(0)=1.28\pm0.02$. Lines serve as a guide for the eyes. Time is given in reduced units as discussed in the text.

$$\frac{k_BT}{V}\zeta_0 = \int_0^\infty\langle\overset{\text{os}}{\mathbf{Q}}_{\alpha\beta}(0)\overset{\text{os}}{\mathbf{Q}}_{\alpha\beta}(t)\rangle dt = \int_0^\infty C_{\zeta_0}(t)dt,$$

$$\frac{k_BT}{V}\zeta_r = \int_0^\infty\langle\overset{\text{a}}{\mathbf{Q}}_{\alpha\beta}(0)\overset{\text{a}}{\mathbf{Q}}_{\alpha\beta}(t)\rangle dt = \int_0^\infty C_{\zeta_r}(t)dt. \tag{26}$$

To improve the statistics, it is common to make averages over all independent $\alpha\beta$ autocorrelation functions. However, we here monitor each correlation function individually since finite-size and anisotropy effects on the autocorrelation functions may be averaged out by this procedure. The anisotropy is, furthermore, quantified by the order parameter, s, which is the largest eigenvalue of the order tensor:

$$\mathbf{S} = \frac{3}{2N_{\text{mol}}}\left[\sum_i\hat{\mathbf{u}}_i\hat{\mathbf{u}}_i - \frac{1}{3}\mathbf{I}\right]. \tag{27}$$

$\hat{\mathbf{u}}_i$ is the unit vector parallel to the main molecular axis of molecule i. For isotropic fluids $s=0$ whereas for $|s|=1$ the molecules are perfectly aligned.

IV. MOLECULAR-DYNAMICS RESULTS

To our knowledge only Evans and Streett [19] have calculated the spin viscosities using molecular-dynamics simulations. In this work the authors simulated a molecular nitrogen fluid with mass density $\rho=1.244$ and $T_m=2.10$ giving a pressure $p\approx0$ (in reduced units as mentioned earlier). They applied a slightly different molecular model where the bond length was fixed at $l_b=0.3292$ rather than allowing for bond vibrations. In order to obtain the same zero pressure we have here used $\rho=1.065$ and $T_m=2.10$. The normalized autocorrelation functions of $C_{\eta_0}(t)$, $C_{\eta_r}(t)$, $C_{\zeta_0}(t)$, and $C_{\zeta_r}(t)$ are plotted in Fig. 1. They are very similar to the correlation functions calculated by Evans and Streett (their Figs. 2, 3, 5, and 6). The corresponding viscosities are listed in Table I, where we have compared the data from Evans *et al.* with our data. It is seen that the shear and rotational viscosities are the same within statistical error noting that our pressure is slightly

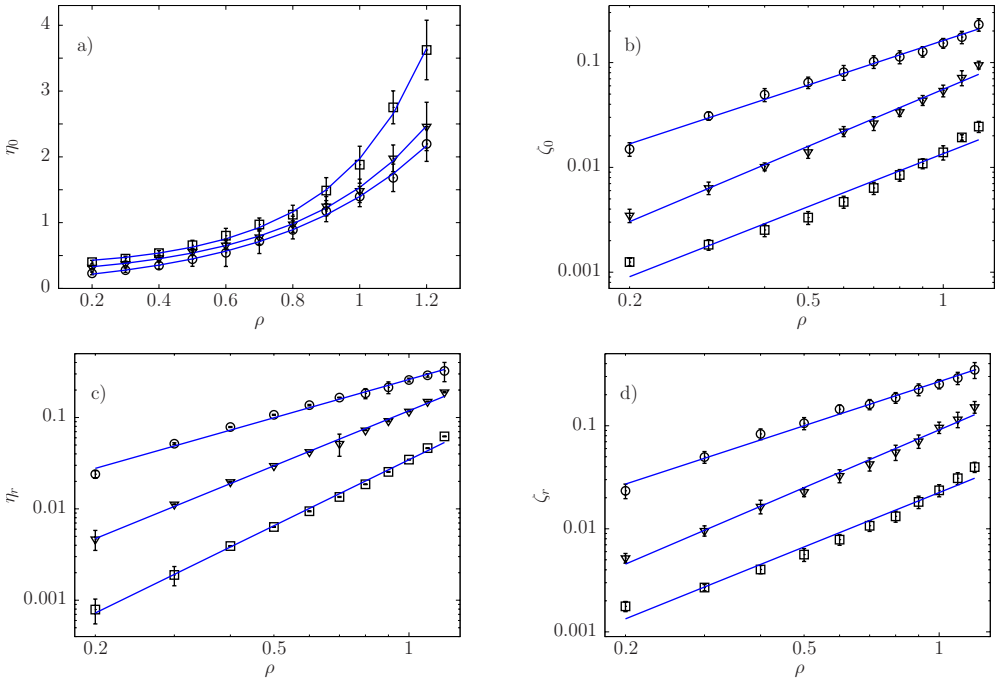

FIG. 2. (Color online) η_0, ζ_0, η_r, and ζ_r as functions of mass density ρ for N_s=2 (squares), 3 (triangles), and 4 (circles). Notice the double logarithmic scales in (b)–(d). In (a) the lines represent the best fits of the stretched exponential function to the data and for (b)–(d) power-law fits. The quantities are given in reduced units as discussed in the text.

lower than zero. However, the spin viscosities have values that are orders of magnitude different. This large discrepancy is not likely to be a result of the different models nor the fact that the thermodynamical properties are slightly different. It would be most interesting to have one of these results independently verified.

With this in mind, we now return to the study of the more general fluids as described in Sec. III. To this end, we carry out a series of simulations for different densities varying the number of UAU, N_s, from 2 to 4 keeping the temperature fixed at $T \approx 4.25$ using system sizes of N_{mol}=864, 576, and 432, respectively. For lower temperatures the order parameter reveals that the system becomes anisotropic and for smaller system sizes we have observed finite-size effects on the autocorrelation functions for N_s=4. Figure 2 summarizes the four viscosities as a function of density for the three different molecular fluids investigated. For the shear viscosity we have fitted the data to the stretched exponential function,

$$\eta_0(\rho) = Ae^{\lambda\rho^{\beta}}, \tag{28}$$

using A, λ, and β as fitting parameters. This functional form for the density-dependent viscosity has also been successfully applied to atomic systems [32]. From Figs. 2(b)–2(d) it is observed that ζ_0, η_r, and ζ_r approximately follow a power law in the density region studied here. Notice, however, that for N_s=2 and N_s=3 the deviation from the power law is systematic. We have not been able to find a functional form that fitted the data better than a simple power function. It is also interesting to note that the shear viscosity is larger for small molecules, whereas the spin and rotational viscosities increase with increasing N_s. The reason for this is due to the fact that for constant mass density the average distance between UAU not belonging to the same molecule increases for increasing N_s. This is also manifested in a decrease in pressure as it can be seen in Table II. From Fig. 2 we also observe that the spin viscosities do not change dramatically for small density variations or equivalently small pressure variations. This underlines what was mentioned earlier: the small pressure difference between Evans and Streett's simulations and our simulations cannot explain the order of magnitude difference observed in the spin viscosities.

The autocorrelation formalism provides a convenient way of evaluating the frequency dependence of the transport coefficients. The complex shear viscosity, for example, is given by the one-sided Fourier transform [20]:

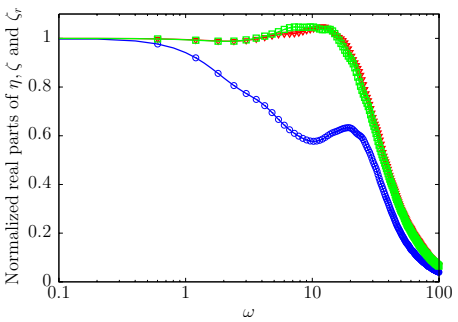

FIG. 3. (Color online) η' (circles), ζ' (squares), and ζ_r' (triangles) as functions of ω for N_s=4 and ρ=0.2. The functions have been normalized with respect to their ω=0 values. The frequency is given in reduced units as discussed in the text.

TABLE I. Comparison of data between Evans and Streett [19] (shear and spin viscosities), Evans and Hanley [4] (rotational viscosity), and this work. The quantities are given in reduced units as discussed in the text.

	ρ	T	p	η_0	ζ_0	η_r	ζ_r
Evans, Streett and Hanley	1.244	2.10 ± 0.02	0.00 ± 0.03	2.5 ± 0.7	0.7 ± 0.2	0.045 ± 0.01	0.6 ± 0.2
This work	1.065	2.14 ± 0.06	-0.4 ± 0.3	2.2 ± 0.2	0.014 ± 0.001	0.033 ± 0.001	0.023 ± 0.002

$$\tilde{\eta}(\omega) = \eta'(\omega) + i\eta''(\omega) = \frac{V}{k_B T}\int_0^\infty \langle \overset{\text{os}}{\mathsf{P}}_{\alpha\beta}(0)\overset{\text{os}}{\mathsf{P}}_{\alpha\beta}(t)\rangle e^{-i\omega t}dt, \tag{29}$$

where $\eta'(\omega)$ and $\eta''(\omega)$ are the real and imaginary parts of the viscosity, respectively. Note that $\eta'(0)=\eta_0$ and $\eta''(0)=0$. The one-sided Fourier transform can also be applied in order to evaluate the complex spin viscosities $\tilde{\zeta}(\omega)=\zeta'(\omega)+i\zeta''(\omega)$ and $\tilde{\zeta}_r(\omega)=\zeta_r'(\omega)+i\zeta_r''(\omega)$. This is, however, not the case for the rotational viscosity since this coefficient cannot be evaluated by the traditional Green-Kubo method as discussed above. We will therefore limit the study to investigate $\tilde{\eta}(\omega)$, $\tilde{\zeta}(\omega)$, and $\zeta_r(\omega)$. To remove the effect of the truncation of the autocorrelation function, the data are smoothed with a Hann window [33] to avoid spurious oscillations in the transform as a result of the truncation. We stress that none of the features discussed below are affected by this procedure. In Fig. 3 we have plotted $\eta'(\omega)$, $\zeta'(\omega)$, and $\zeta_r'(\omega)$ as a function of ω where $N_s=4$ and $\rho=0.2$. It is seen that the viscoelastic response of the fluid happens for $\omega>0.3$ and is first manifested in the reduction of η'. The data have been compared with the Maxwell model:

$$\tilde{\eta}(\omega) = \frac{\eta_0}{1+i\omega\tau_M}, \tag{30}$$

where τ_M is the Maxwell relaxation time, but shows poor agreement over the whole ω range. It should be pointed out that using the atomic formalism when evaluating the pressure tensor may result in a different frequency dependence for $\omega>0$ [34]. From Fig. 3 it is also observed that the real part of the spin viscosities both have maxima at around $\omega=10$, that is, there is an increased viscous response from the molecular spin fluxes for $N_s=4$. This maximum disappears for higher densities and is not present for the other fluids studied here, i.e., where $N_s=2$ and $N_s=3$.

V. EFFECT OF MOLECULAR ROTATION ON VELOCITY PROFILES FOR NANOFLOWS

For a fluid confined between two parallel walls that undergoes a steady Poiseuille flow, the extended Navier-Stokes equations are given by Eqs. (4) and (5) with the addition of the production term in the equation for u_x: ρFe. Assuming strictly no-slip boundary conditions, i.e., $u_x(\pm h)=0$ and $\Omega_z(\pm h)=0$ for all time and where h is the location of the walls (i.e., the channel half width), the solution is given by [19,35]

$$u_x(\bar{y}) = u_c\left[1 - \bar{y}^2 + \frac{2\eta_r \coth(Kh)}{(\eta_0+\eta_r)Kh}\left(\frac{\cosh(Kh\bar{y})}{\cosh(Kh)} - 1\right)\right], \tag{31}$$

$$\Omega_z(\bar{y}) = \frac{u_c}{h}\left[\bar{y} - \frac{\sinh(Kh\bar{y})}{\sinh(Kh)}\right], \tag{32}$$

where $\bar{y}=y/h$ and

$$K = \left[\frac{4\eta_0\eta_r}{(\eta_0+\eta_r)(\zeta_0+\zeta_r)}\right]^{1/2} \text{ and } u_c = \frac{\rho F_e h^2}{2\eta_0}. \tag{33}$$

From Eq. (31) it can be seen that if the coupling between the intrinsic angular and translational velocities is ignored Eq. (31) reduces to the traditional solution:

$$u_x^P(\bar{y}) = u_c(1-\bar{y}^2). \tag{34}$$

This means that the relative effect, $u^{\text{rel}}(\bar{y})=u_x(\bar{y})/u_x^P(\bar{y})$, is given directly by

$$u^{\text{rel}}(\bar{y}) = 1 + \frac{1}{1-\bar{y}^2}\frac{2\eta_r \coth(Kh)}{(\eta_0+\eta_r)Kh}\left[\frac{\cosh(Kh\bar{y})}{\cosh(Kh)} - 1\right] \tag{35}$$

for $|\bar{y}|<1$. From this expression it is seen that the relative effect is not dependent on the external force field. Furthermore, since the second term on the right-hand side of Eq. (35) is always negative, the rotation leads to a flow rate reduction. In the following we will use $\sigma=3.8$ Å, $\epsilon/k_B=72$ K, and $m=13$ to model alkenes, i.e., ethene or ethylene ($CH_2=CH_2$), propa-diene ($CH_2=C=CH_2$), and buta-triene ($CH_2=C=C=CH_2$). $u^{\text{rel}}(\bar{y})$ is plotted for different densities and N_s in Fig. 4 using the values of the transport coefficients obtained in Sec. IV. It is observed that the effect of the rotation is very high for large molecules and intermediate densi-

TABLE II. Isotropic pressure, p, for different densities and UAU per molecule, N_s. The pressure is given in reduced units as discussed in the text.

	$\rho=0.5$			$\rho=1$		
N_s	2	3	4	2	3	4
p	0.9 ± 0.2	0.4 ± 0.1	0.08 ± 0.3	4.9 ± 0.6	0.9 ± 0.3	-0.1 ± 0.6

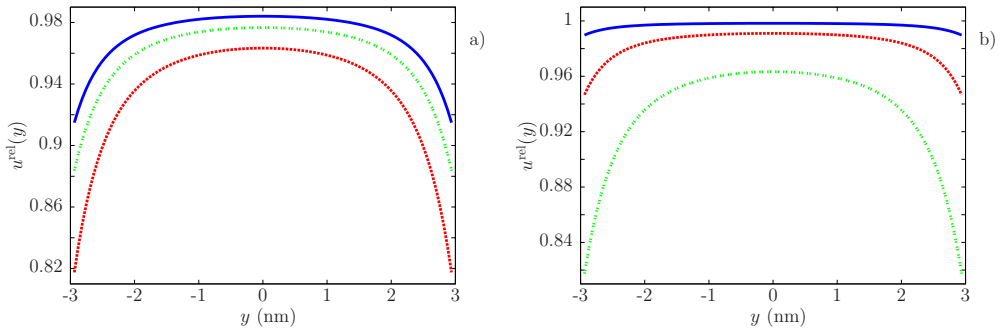

FIG. 4. (Color online) Equation (35) plotted as a function y for different densities and N_s. (a) Buta-triene for $\rho=78.7$ kg m^{-3} (full line), $\rho=236.1$ kg m^{-3} (dotted line), and $\rho=472.1$ kg m^{-3} (dashed line). (b) Ethene (full line), propa-diene (dotted line), and buta-triene (dashed line) for $\rho=236.1$ kg m^{-3}.

ties. It is important to point out the fact that the effect is not always monotonically increasing with respect to density due to the product of the hyperbolic and cotangent functions. It is also seen that the relative effect is largest near the wall. This is due to the very large gradient in the molecular angular velocity in this region, which can be seen from Eq. (32). The effect of the rotation on the flow rate can also be evaluated. To this end we define the flow rates Q and Q^P as $Q=2\int_0^1 u_x(\bar{y})d\bar{y}$ and $Q^P=2\int_0^1 u_x^P(\bar{y})d\bar{y}$ such that for $h>0$:

$$\frac{Q^P-Q}{Q^P}=\frac{3\eta_r[\coth(Kh)-1]}{(\eta_0+\eta_r)(Kh)^2}. \tag{36}$$

As depicted in Fig. 5, Eq. (36) is a decreasing function with respect to h, that is, the flow rate difference increases as the channel width decreases. For the values of the transport coefficients used in Fig. 5 the flow rate can be reduced by around 10% for a slit pore with a width of 2 nm. Such highly confined geometries can be found in flows through carbon nanotubes [36] and the coupling between intrinsic angular and linear velocities is, therefore, extremely relevant in such cases. Figure 5 shows the maximum effect of the molecular rotation for all fluids investigated here. The fact that there is an effect is in agreement with the characteristic length, l_c, which is 0.50 nm for buta-triene at $\rho=236.1$ kg m^{-3}.

The predicted flow rate reduction, Eq. (36), can be compared with direct nonequilibrium molecular-dynamics (direct-NEMD) simulations. In such simulations large inhomogeneities are present at the wall fluid interface and also the isotropic assumption is no longer justified [37]. These problems can be overcome by comparing the velocity profiles away from the wall forcing the continuum solution to satisfy boundary conditions specified by the direct-NEMD data. Thus, ignoring the coupling the continuum problem is formulated as $\partial^2 u_x^P/\partial y^2=-\rho F_e/(2\eta_0)$ subjected to the boundary conditions $u_x^P(\pm h')=u_0$ giving

$$u_x^P(y)=\frac{\rho F_e h'^2}{2\eta_0}(1-\bar{y}^2)+u_0, \tag{37}$$

where h' is a point in the channel sufficiently far away from the walls and u_0 is the corresponding streaming velocity at that point found from the direct-NEMD simulations. The NEMD method is described in detail elsewhere [15] and we will not go into detail here, but note that the wall fluid interactions are governed by the Weeks-Chandler-Andersen potential [38], to prevent excessive condensation of the fluid on the wall surface. Figure 6 compares the simulation data with Eq. (37) for a buta-triene fluid at $\rho=196.7$ kg m^{-3} and $T=306$ K where the channel half width is around 2.25 nm. $h'=1.15$ nm which is the point where the density is constant. The flow reduction is 4.1% compared with the predicted 5.3%, Eq. (36).

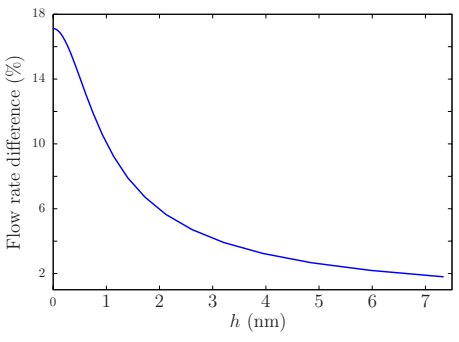

FIG. 5. (Color online) Flow rate difference as function of h for buta-triene with $\rho=236.1$ kg m^{-3}.

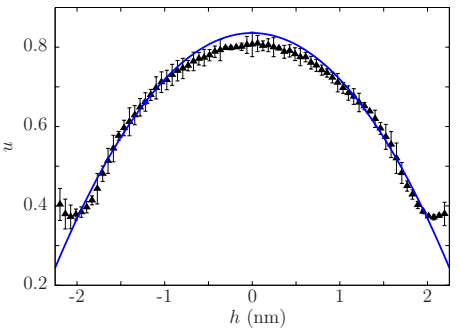

FIG. 6. (Color online) Comparison of direct-NEMD data (triangles) with Eq. (37) (full line) for a buta-triene fluid at $\rho=196.7$ kg m^{-3} and $T=306$ K. $h'=1.15$ nm. Errors are given as half the maximum difference of five runs. The velocity is given in reduced units as discussed in the text.

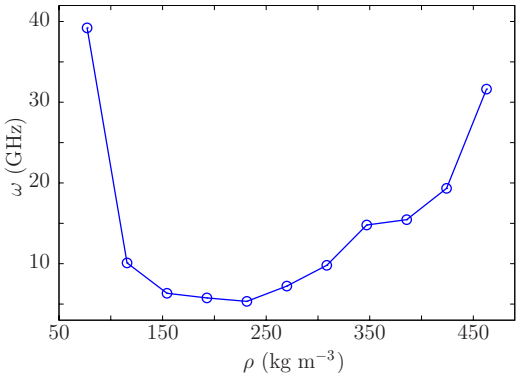

FIG. 7. (Color online) External force field frequency required for $\epsilon=1\times10^{-3}$ for buta-triene. The line serves as a guide for the eyes.

For liquid nitrogen undergoing a Poiseuille flow the values of the transport coefficients obtained by Evans *et al.* predict that the flow rate is reduced by around 14% for a 2 nm channel. This can be compared with our prediction of a 0.65% flow rate reduction. As discussed above, our predictions are close to the NEMD results indicating that the spin viscosities are lower than what is given by Evans and Streett giving a smaller, but nevertheless very important, effect of the coupling.

According to Eq. (12) we can estimate the effect caused by molecular moment of inertia for an oscillatory flow. For buta-triene at $\rho=314$ kg m^{-3} confined between a 2-nm-wide slit pore the frequency required to obtain a 1% flow rate reduction is

$$\sqrt{\frac{\varepsilon h \nu_0^{3/2}}{\Theta \nu_r}} \approx 9 \text{ GHz}. \tag{38}$$

Note that this is actually orders of magnitude smaller than the characteristic frequency, ω_c, but it is well within the purely viscous regime; see Fig. 3. Thus, the inertia effect is small compared with the effect from angular momentum diffusion when the channel is sufficiently small. We have summarized the results for buta-triene for different densities where $h=1$ nm and $\varepsilon=1\times10^{-3}$ in Fig. 7.

VI. CONCLUSION

In this paper we presented equilibrium molecular-dynamics results for the shear, rotational, and spin viscosities for different linear molecular fluids. It was found that the density dependence of the shear viscosity follows a stretched exponential function, whereas the rotational and spin viscosities approximately follow a power law. For the shear and rotational viscosities this is in agreement with earlier findings [22]. The frequency-dependent shear and spin viscosities were also investigated via the one-sided Fourier transform of the relevant autocorrelation functions. It was found that viscoelastic behavior of the fluid is first manifested in the shear viscosity. Interestingly, the real part of the spin viscosities features a maximum for nonzero frequency for low densities and $N_s=4$, thus, enhancing the viscous response of the fluid in this region.

Using the calculated transport coefficients and thereby assuming isotropy and homogeneity the effect of the coupling between the molecular rotation and linear momentum was investigated for fluids in highly confined geometries. It was shown that the flow rate is reduced significantly for sufficiently small channel widths: for buta-triene as much as 10% for a 2 nm channel which is obtainable with today's nanotechnology [36]. The coupling effect decreases rapidly with increasing channel width and the flow rate difference is less than 1% for a 20-nm-wide channel. We also showed that for an oscillatory flow extremely high frequencies are required if any effect from the molecular rotational inertia is to be observed. This effect may be significant for larger molecules. Once again we stress that the results for the spin viscosities were found to be one order of magnitude smaller than those earlier by Evans and Streett [19]. As stated in Sec. IV it is very important to have a third independent study confirming one of these studies.

In must also be stressed that we have only investigated the effect of the molecular rotation for isotropic fluids. At the wall fluid interface it is well known that the molecules tend to align with the wall [37]. For molecules with lengths comparable with the channel width geometric constraints may likely influence the overall fluid dynamics. We have also assumed that the system is homogeneous such that transport coefficients are assumed to be constants. This assumption is not strictly true since the density features large variations in the wall fluid interface region; see, e.g., Ref. [39]. Interestingly these large variations do not influence the fluid dynamical properties greatly as long as the channel width is more than 6–7 molecular diameters [40]. Finally, the no-slip boundary condition imposed on the extended Navier-Stokes equations is not necessarily true, in that very large slippage can occur in nanofluids [41]. No-slip boundary conditions can be obtained by allowing strong attraction between the wall atoms and fluid molecules compared with the fluid-fluid interaction. Nevertheless, the effect of the coupling on the velocity profile is independent of whether no-slip or slip boundaries are used.

It is interesting that many research groups worldwide are currently focusing on the breakdown of the no-slip boundary condition for nanoflows. This phenomenon is believed to be one of the mechanisms behind the enhanced flow through carbon nanopores; see, e.g., Ref. [36]. However, as we have shown in this paper the coupling between the intrinsic angular momentum and linear momentum has the opposite effect, reducing the flow rate. Thus, in order to correctly predict the flow rate through nanopores this potentially very large effect must also be considered.

ACKNOWLEDGMENTS

The authors would like to thank the Australian Research Council for supporting this work as a part of Discovery Grant No. DP 0663759. Also, we wish to acknowledge the referees for their valuable comments.

[1] C. F. Curtiss, J. Chem. Phys. **24**, 225 (1956).
[2] S. R. de Groot and P. Mazur, *Nonequilibrium Thermodynamics* (Dover, Mineola, NY, 1984).
[3] R. F. Snider and K. S. Lewchuk, J. Chem. Phys. **46**, 3163 (1967).
[4] D. J. Evans and H. J. M. Hanley, Phys. Rev. A **25**, 1771 (1982).
[5] M. Born, Z. Phys. **1**, 221 (1920).
[6] H. Grad, Commun. Pure Appl. Math. **5**, 455 (1952).
[7] N. K. Ailawadi, B. J. Berne, and D. Forster, Phys. Rev. A **3**, 1462 (1971).
[8] H. Kneppe, F. Schneider, and N. K. Sharma, J. Chem. Phys. **77**, 3203 (1982).
[9] R. Edberg, D. J. Evans, and G. P. Morriss, Mol. Phys. **62**, 1357 (1987).
[10] S. Sarman and D. Evans, J. Chem. Phys. **99**, 9021 (1993).
[11] S. Sarman, J. Chem. Phys. **108**, 7909 (1998).
[12] K. P. Travis, B. D. Todd, and D. J. Evans, Physica A **240**, 315 (1997).
[13] K. P. Travis and D. J. Evans, Phys. Rev. E **55**, 1566 (1997).
[14] J. Delhommelle, Mol. Phys. **100**, 3479 (2002).
[15] J. S. Hansen, B. D. Todd, and P. J. Daivis, Phys. Rev. E **77**, 066707 (2008).
[16] J. S. Hansen, P. J. Daivis, and B. D. Todd, Microfluid. Nanofluid. **6**, 785 (2009).
[17] B. Hinds, N. Chopra, T. Rantell, R. Andrews, and V. G. L. Bachas, Science **303**, 62 (2004).
[18] K. R. Schumacher, I. Sellien, G. S. Knoke, T. Cadar, and B. A. Finlayson, Phys. Rev. E **67**, 026308 (2003).
[19] D. J. Evans and W. B. Streett, Mol. Phys. **36**, 161 (1978).
[20] J. P. Hansen and I. R. McDonald, *Theory of Simple Liquids* (Academic, London, 1986).
[21] N. Allinger, J. Am. Chem. Soc. **99**, 8127 (1977).
[22] R. J. D. Moore, J. S. Hansen, and B. D. Todd, J. Phys. Chem. **128**, 224507 (2008).
[23] T. A. Hunt, Ph.D. thesis, Swinburne University of Technology, 2008.
[24] J. H. R. Clarke, in *Computer Modeling of Fluids, Polymers and Solids*, NATO Advanced Studies Institute: Series C, Vol. 293, edited by C. R. A. Catlow, S. C. Parker, and M. P. Allen (Kluwer Academic, Dordrecht, 1990).
[25] D. Rapaport, *The Art of Molecular Dynamics Simulation* (Cambridge University Press, Cambridge, 1995).
[26] D. Frenkel and B. Smit, *Understanding Molecular Simulation* (Academic, London, 1996).
[27] S. Nosé, Mol. Phys. **52**, 255 (1984).
[28] W. G. Hoover, Phys. Rev. A **31**, 1695 (1985).
[29] B. D. Todd and P. J. Daivis, Mol. Simul. **33**, 189 (2007).
[30] R. Zwanzig, J. Chem. Phys. **40**, 2527 (1964).
[31] B. Berne, J. Boon, and S. Rice, J. Chem. Phys. **45**, 1086 (1966).
[32] B. D. Todd, Phys. Rev. E **72**, 041204 (2005).
[33] W. Press, W. Vettering, S. Teukolsky, and B. Flannery, *Numerical Recipes in C* (Cambridge University Press, Cambridge, 1992).
[34] M. P. Allen, Mol. Phys. **52**, 705 (1984).
[35] A. C. Eringen, *Proceedings: Contribution to Mechanics* (Pergamon, New York, 1969).
[36] D. S. Sholl and J. K. Johnson, Science **312**, 1003 (2006).
[37] *Monte Carlo and Molecular Dynamics Simulations in Polymer Science*, edited by K. Binder (Oxford University Press, New York, 1995).
[38] J. D. Weeks, D. Chandler, and H. C. Andersen, J. Chem. Phys. **54**, 5237 (1971).
[39] S. Toxvaerd, J. Chem. Phys. **74**, 1998 (1981).
[40] K. P. Travis, B. D. Todd, and D. J. Evans, Phys. Rev. E **55**, 4288 (1997).
[41] J. Koplik, J. Banavar, and J. Willemsen, Phys. Fluids A **1**, 781 (1989).